Wavelength-Selective $1 \times K$ Switches Using Free-Space Optics and MEMS Micromirrors: Theory, Design, and Implementation

Dan M. Marom, *Member, IEEE*, David T. Neilson, *Senior Member, IEEE, Member, OSA*, Dennis S. Greywall, Chien-Shing Pai, Nagesh R. Basavanhally, Vladimir A. Aksyuk, Daniel O. López, Flavio Pardo, Maria Elina Simon, Yee Low, Paul Kolodner, and Cristian A. Bolle

***Abstract*—The design and performance of several generations of wavelength-selective $1 \times K$ switches are reviewed. These optical subsystems combine the functionality of a demultiplexer, per-wavelength switch, and multiplexer in a single, low-loss unit. Free-space optics is utilized for spatially separating the constituent wavelength division multiplexing (WDM) channels as well as for space-division switching from an input optical fiber to one of K output fibers ($1 \times K$ functionality) on a channel-by-channel basis using a microelectromechanical system (MEMS) micromirror array. The switches are designed to provide wide and flat passbands for minimal signal distortion. They can also provide spectral equalization and channel blocking functionality, making them well suited for use in transparent WDM optical mesh networks.**

***Index Terms*—Gratings, microelectromechanical devices, microelectromechanical system (MEMS), optical add/drop multiplexing (OADM), optical filters, optical switches, wavelength-selective switch.**

I. Introduction

TRANSPARENT switching, where the optical signal does not undergo conversion to the electrical domain for switching purposes, can greatly simplify and reduce the cost of implementing optical networks by the elimination of optical to electrical to optical (OEO) conversions [1], [2]. The use of transparent switching within wavelength division multiplexed (WDM) systems further necessitates that switches be either wavelength-selective or be preceded by a demultiplexer and followed by a multiplexer for channel access [3]. The former is typically more desirable in many switching scenarios, since it avoids multiple components and will typically have lower losses and wider passbands. At an optical add/drop multiplexer (OADM) node, a subset of the optical channels, or wavelengths, propagating in the optical fiber is extracted for local detection (known as drop channels) and new optical channels are inserted in their place (known as add channels). The optical add/drop functionality can be achieved by the use of a channel blocking filter [4]–[6] placed between a passive splitter (for dropping channels) and a passive combiner (for adding channels). The device blocks the dropped channels from continuing to propagate in the line system and interfering with the added channels. A more efficient solution utilizes a wavelength-selective 2×2 switch [7], [8]. This switch has two inputs, the line system input, and the add channels and two outputs, the line system output, and the drop channels. These wavelength-selective switches use internal switching elements to route the individual WDM channels to the proper port.

As optical networks evolve from simple ring architecture with OADM nodes to optical mesh networks [1], the transparent switching requirements change. Mesh network nodes are typically linked to three or four neighboring nodes with each link carrying two-way traffic. Transparent switching at each node's network links, or cross connect functionality, is required for implementing an all-optical network. Furthermore, a modular cross connect fabric may be more desirable from an economic standpoint, as the node interconnecting links are deployed gradually. Finally, the cross connect may be required to support a power equalization feature [9] for optimal optical transport.

The wavelength-selective $1 \times K$ switch fulfills all the mesh networking requirements above [10]–[15]. The switch has a single input fiber that carries the WDM signal consisting of N channels, and distributes these N channels in a reconfigurable and independent fashion across the K output fibers. The switches [10]–[14] use a microelectromechanical system (MEMS) mirror array for the beam steering elements. Owing to the reciprocal nature of light propagation, the same switch fabric may be operated in reverse for wavelength-selective $K \times 1$ switching functionality. A complete wavelength-selective $K \times K$ cross connect (K WDM inputs and K WDM outputs) is implemented by utilizing K switch modules and K passive splitters [16]. A wavelength-selective $K \times K$ cross connect can also be constructed using blocking filters [5], [6], [17], but has additional loss since it requires both passive splitting and combining and further requires K^2 blocking filters component count.

In this paper, we review the technology of the wavelength-selective $1 \times K$ switch, from design choices and tradeoffs, through a description of various switch implementations we constructed,

Manuscript received June 7, 2004; revised January 7, 2005.

D. M. Marom and D. T. Neilson are with Bell Laboratories, Lucent Technologies, Holmdel, NJ 07733 USA (e-mail: dmarom@lucent.com).

D. S. Greywall, C. S. Pai, N. R. Basavanhally, V. A. Aksyuk, D. O. López, F. Pardo, M. E. Simon, Y. Low, P. Kolodner, and C. A. Bolle are with the Bell Laboratories, Murray Hill, NJ 09999 USA.

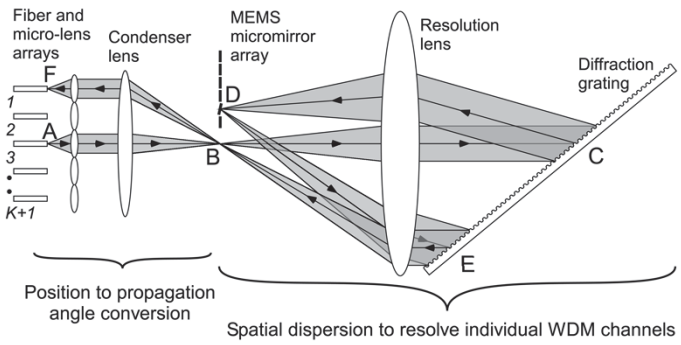

Fig. 1. Optical system configuration for wavelength-selective switch. The system is composed of a subsystem that converts fiber position to angle and a second subsystem, which uses a lens and diffraction grating to provide spatial dispersion to separate the channels.

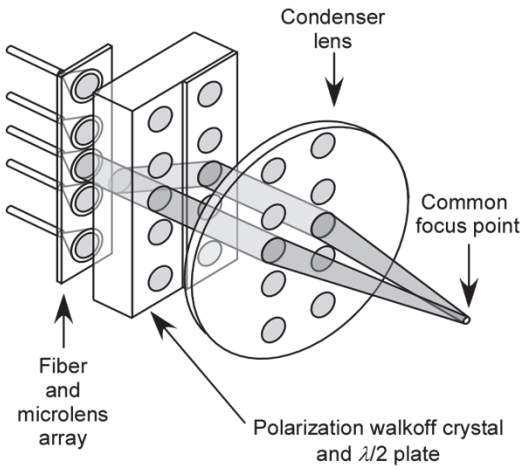

Fig. 2. Position to angle subsystem showing unequal spacing of fibers and lenses to introduce gaps for the variable attenuation function and polarization diversity optics.

II. Design of Wavelength-Selective $1 \times K$ Switches

The wavelength-selective $1 \times K$ switch design is based on the guiding principle of optical imaging, leading to simple assembly and alignment. The optical system partitions the aperture to provide for multiple ports [7] and uses a coaxial relay imaging system to map the input beams onto the MEMS micromirror array and back. The coaxial arrangement facilitates assembly and packaging, as all elements are aligned along one-dimensional space, and can be housed in a robust tubular holder (symmetric structure with no weak bending axis). It is useful to consider the switch to be comprised of two major subassemblies (Fig. 1). The role of the first subassembly is to image the input and output optical fiber end faces onto a common magnified spot B. This subassembly converts the distinct spatial locations of the fibers to unique angular propagation directions at position B. A tilting mirror could be placed at this image plane to reflect the light and implement a nonwavelength-selective $1 \times K$ switch [18]. Here the light originating from the input fiber A would be imaged on the desired output fiber F. Attenuation level control can be obtained by deliberately misaligning the image location from the output fiber, by tilting this mirror away from the ideal coupling angle. The second subassembly introduces the desired wavelength-selectivity property. It spatially disperses the input magnified common spot, consisting of the N WDM channels, onto the MEMS micromirror array, such that each channel is imaged upon a separate mirror in the array for independent addressing. Each micromirror in the array is tilted to a desired angle, which determines the output fiber to which the reflected light will couple upon imaging back to the fiber array, on a WDM channel basis. A typical beam path in the switch originates from the input fiber A and is imaged with magnification to B by the first subassembly. The second subassembly images one of the WDM channels from B to D, according to wavelength. The micromirror at D is tilted to a prescribed angle, and the reflected light that is propagating in a new direction is imaged back to point B by the second subassembly. Finally, the first subassembly images the reflected signal to the output fiber location F by a last imaging operation.

Due to the independent imaging operations each subassembly performs, we may analyze the operation of each subassembly reach each output fiber. The second subassembly determines the amount of spatial dispersion for separating the WDM channels and obtaining the necessary passband width. We will establish the characteristics of each subassembly, as well as the overall design tradeoffs of the wavelength-selective switch.

A. Position-to-Propagation Angle Subassembly

The optical subassembly responsible for imaging the optical fiber end faces onto a common magnified spot is comprised of a fiber array, a matching microlens array, polarization diversity optics, and a condenser lens whose aperture subtends all the beam apertures from the fibers (Fig. 2). The fiber array consists of $K + 1$ fibers, where one fiber is assigned to carry the input signal, and the remaining K fibers are the output fibers. The optical axes of the individual lenses and fibers are coaxially aligned and arranged in a one-dimensional array to accommodate mirrors with a single tilt axis. Furthermore, the fibers and lenses are placed on an irregularly spaced grid to introduce gaps between some of the lens apertures. This supports the attenuation function without giving rise to crosstalk. We also employ a polarization-diversity solution to eliminate the polarization sensitivity of the diffraction grating employed in the second optical subassembly. The polarization diversity is provided by an anisotropic uniaxial crystal and a half-wave plate. The uniaxial crystal separates an input beam into two distinct (non overlapping), copropagating, orthogonally polarized beams. The half-wave plate rotates the polarization state of one of the beams such that the two beams are copolarized. The two beams propagate within the optical subsystem, and are merged back to a single-beam before coupling to the selected output fiber by the waveplate and uniaxial crystal combination. Due to the imaging operation, the two beams exchange their positions in the return path toward the output fibers. Thus, path length differences between the two beams, as experienced by the beam traversing the half-wave plate, are compensated in the return path. This ensures that the system will also have low polarization mode dispersion (PMD).

array (focal length f_1) and the condenser lens (focal length f_2). The imaging operation magnifies the optical beam emerging from the single mode fiber by factor $M = f_2/f_1$. The $F\#$ of the lenses in the microlens array are matched to the optical beam's numerical aperture (NA). Using a Gaussian beam waist of 10.5 μm for the beam from a single-mode fiber, the lens $F\#$ should be at most 3.5 to prevent significant beam clipping ($< 1\%$). It is desirable to pack the microlenses in the lens array as tightly as possible, to keep the $F\#$ of the condenser lens as large as possible. At minimum, the microlens pitch will equal the individual lens diameter, D_L, and the condenser lens aperture is, therefore, $D_L(K+1)$. However, for implementing the spectral equalization functionality, increased spacing between microlenses is required to allow for attenuation by beam displacement for intentional imperfect coupling to the output fiber. To conserve the condenser lens aperture, the intermicrolens spacing, or gaps, are inserted between every pair of microlenses. This ensures that there is a gap available to only one side of each microlens in the array for attenuation by beam displacement, and a total of $K \div 2$ gaps, where the symbol $\div$ denotes the div operation.

The intermicrolens spacing, or gap size, is determined from the required attenuation dynamic range and minimum crosstalk requirements. At the maximal attenuation setting required, we must still suppress the crosstalk to the adjacent output fiber. We define the microlens pitch at locations where a gap is inserted as P_L (Fig. 3). The gap size is, therefore, $P_L - D_L$. For a given beam shift x_0 from the microlens optical axis, the attenuation to the desired output fiber and the crosstalk to the neighboring fiber is calculated by the power overlap integral [19], yielding

$$\eta_{\text{attenuation}}(x_0) = \left| \int_{\text{lens aperture}} \Psi(x,y)\Psi(x - x_0, y)\, dxdy \right|^2 \quad (1)$$

and

$$\eta_{\text{crosstalk}}(x_0) = \left| \int_{\text{lens aperture}} \Psi(x,y)\Psi(x + P_L - x_0, y)\, dxdy \right|^2 \quad (2)$$

where the collimated beam profile is denoted by $\Psi(x,y)$. Note that the finite extent of the microlens aperture assists in the attenuation functionality, as a fraction of the beam power is lost. In our designs, the criteria are for 10-dB attenuation range while maintaining crosstalk below 40 dB. Using a Gaussian beam approximation for the beam profile and microlenses of $F\# = 3.5$, then the necessary pitch P_L is approximately 1.5 times the lens diameter D_L (or gap size is one half the lens diameter).

The condenser lens aperture with added gaps of half diameter size is, therefore, $D_L(K+1) + (D_L/2)(K \div 2)$. Given the condenser lens aperture and focal length, we can now evaluate its $F\#$ as

$$F\#_{\text{cond}} = \frac{F\#_{\mu\text{lens}} M}{\frac{K+1+(K\div 2)}{2}} \approx \frac{F\#_{\mu\text{lens}} M}{\frac{5K}{4+1}}. \quad (3)$$

The condenser lens $F\#$ decreases as the magnification factor

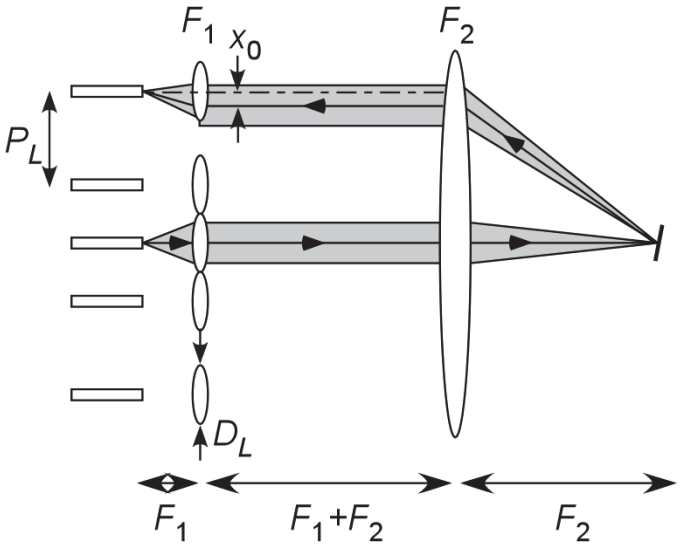

Fig. 3. Position-to-angle conversion optics showing configuration of optics for providing variable attenuation function while maintaining maximum density. The displacement of the beam x_0 causes attenuation by changing the coupling angle at the fiber.

ality, no gaps are required, and the denominator of (3) simplifies to $K+1$. Since K is determined by the required functionality, the only free parameter available for the designer is the magnification factor. A high magnification factor would be desirable for implementing the condenser lens. This would also reduce the mirror tilt angle ranges. If the input fiber is in the middle of the fiber array, as in Figs. 1 and 3, then the mirror must tilt roughly within the range $\pm 1/(4F\#_{\text{cond}})$, in radians. Alternatively, the input fiber may be at the edge of the array, requiring the mirror to tilt in only one direction but at a doubled range of $1/(2F\#_{\text{cond}})$. However, as the magnification ratio M increases, the resulting mode size at the output of the first subassembly also increases. This places a burden on the second subassembly responsible for the spectral resolution, as described in Section II-B.

B. Spatial Dispersion Subassembly

The second optical subassembly spatially disperses the magnified mode that was generated by the first subassembly and images it on the micromirror array. Its design is similar to a spectrometer with a Littrow mounted grating. A single lens collimates the light that is then incident on the grating. The diffracted light, which is propagating back toward the lens and is angularly dispersed, is imaged by the same lens onto the micromirror array. As is well known from classical spectrography, the spectral resolution of the instrument increases with increasing focal length and grating frequency, and with decreasing input slit size. In our switch, the magnified mode size is equivalent to a spectrograph slit size. Therefore, it is desirable to minimize the spot size (decrease M) for obtaining high spectral resolution.

The spatial dispersion, expressed in meters per hertz, provided by the second subassembly is given by [20]

$$\frac{dx}{d\nu} = \frac{2\lambda_0 f_3 \tan(\phi)}{c} \quad (4)$$

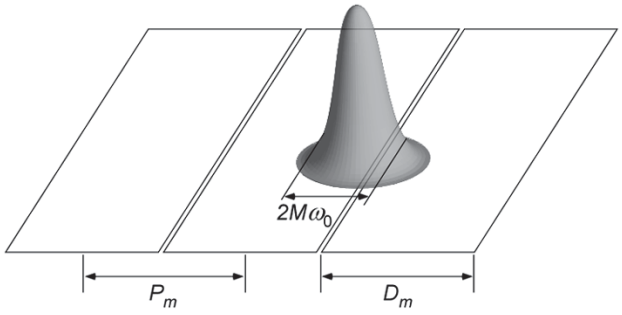

Fig. 4. Schematic of magnified Gaussian mode at a single frequency component imaged on the mirrors of width D_m and pitch P_m. Mode size is M times larger than the output of a single mode fiber, $2\omega_0$, where M is the magnification factor of the imaging system.

the Littrow grating mounting angle. The Littrow angle is given by $\sin(\phi) = \lambda_0 \nu_g / 2$, where ν_g is the grating spatial frequency (in m^{-1}). Therefore, the mirror pitch of the micromirror array will be $P_m = \nu_{\mathrm{ch}} \cdot dx/d\nu$, where ν_{ch} is the WDM channel frequency spacing (in Hz). Note that we are assuming constant spatial dispersion across the total bandwidth of the optical system. In reality, especially for gratings of high spatial frequency, the mirror pitch will not be constant due to the wavelength dependence in the grating diffraction formula [20].

The spatially dispersed image of the magnified Gaussian mode, Fig. 4, present on the micromirror array can be expressed as

$$\varphi(x,y,\nu) = \sqrt{\frac{2}{\pi M^2 \omega_0^2}} \exp\left[-\frac{\left(\frac{x - P_m \nu}{\nu_{\mathrm{ch}}}\right)^2 + y^2}{(M\omega_0)^2} \right] \tag{5}$$

where ω_0 is the Gaussian mode field radius of the beam from a single mode fiber (5.25 μm). The term $P_m \nu / \nu_{\mathrm{ch}}$ in (5) defines the center location of the magnified Gaussian mode as a function of the temporal frequency. The dimensionless ratio ξ of mirror size to the magnified Gaussian mode size $\xi = P_m/(M2\omega_0)$ measures how well the Gaussian mode is confined within the micromirror, and will be shown to determine the passband performance. The frequency-dependent, power-coupling efficiency integral is calculated by performing the traditional overlap integral over the extent of a single mirror at the device plane [19]. More elaborate modeling taking into account the effect of the neighboring mirror states has been performed elsewhere [21]. With the simple model, the coupling efficiency is defined by

$$\begin{aligned} \eta(\nu) &= \left| \int_{y=-\infty}^{\infty} \int_{x=-D_m/2}^{D_m/2} \varphi(x,y,\nu)^2 dx dy \right|^2 \\ &= \frac{1}{4} \left\{ \mathrm{erf}\left[\sqrt{2}\xi \left(\frac{D_m}{P_m} - \frac{2\nu}{\nu_{\mathrm{ch}}} \right) \right] \right. \\ &\qquad \left. + \mathrm{erf}\left[\sqrt{2}\xi \left(\frac{D_m}{P_m} + \frac{2\nu}{\nu_{\mathrm{ch}}} \right) \right] \right\}^2 \end{aligned} \tag{6}$$

where D_m is the physical width of the micromirror in the spatial dispersion direction, and the mirror is modeled as infinite in the orthogonal direction. The mirror size D_m is slightly smaller

simple expressions for the passband and stopband widths of a WDM channel using (6) with the approximation that the contribution of the second error function is constant, which is valid when designing for flat and wide passbands. The passband width ν_{pass} normalized by the channel spacing and measured at η transmissivity level (a characteristic level is $\eta = 0.5$ or -3 dB passband) is defined by

$$\frac{\nu_{\mathrm{pass}}}{\nu_{\mathrm{ch}}} \cong \frac{D_m}{P_m} - \frac{1}{\sqrt{2}\xi} \mathrm{erf}^{-1}\left[\sqrt{4\eta} - 1 \right] \tag{7}$$

where erf^{-1} is the inverse error function. Similarly, the stopband width ν_{block}, originating from crosstalk of neighboring mirrors (or adjacent channels) is

$$\frac{\nu_{\mathrm{block}}}{\nu_{\mathrm{ch}}} \cong 2 - \frac{D_m}{P_m} - \frac{1}{\sqrt{2}\xi} \mathrm{erf}^{-1}\left[1 - \sqrt{4\eta} \right]. \tag{8}$$

The stopband width is typically measured at the $\eta = 10^{-4}$ (-40 dB) level. The two parameters influencing the passband and stopband widths are the fill factor of the array D_m/P_m and the confinement ratio ξ. It is desirable to maximize both bandwidths for minimal signal distortion and crosstalk, which can be satisfied by an increasing confinement ratio ξ. A high fill-factor micromirror array also maximizes the passband width, yet decreases the stopband width. Nevertheless, the mirror arrays are typically fabricated with minimal gap size as technically feasible for maximizing the passband width. In the limiting case of $D_m \to P_m$, the fill-factor approaches 1 and the confinement parameter ξ is the only parameter determining the passband shape, controlling the extent of the passband flatness and the roll-off rate (Fig. 5). Thus, passband requirements can be accommodated by varying the ratio of the mirror size to the magnified Gaussian mode size, which sets ξ.

The available degrees of freedom remaining in designing the second optical subassembly is choice of diffraction grating and lens focal length. For obtaining high spectral resolution within a small package, it is always desirable to select a high spatial frequency diffraction grating. Other factors influencing the grating selection process are the diffraction efficiency and polarization dependence in the telecom (1500–1620 nm) wavelength range. We employ polarization diversity in our switch, implemented in the first subassembly, as the chosen grating does have significant polarization dependence. Once the magnification factor and diffraction grating have been selected, the focal length f_3 of the resolution lens can be established to meet the passband performance metrics. The lens's $F\#$ is equal to the condenser's, as evaluated by (3). However, this lens has a field of view diameter determined by the physical extent of the micromirror array, or $N \cdot P_m$. These two requirements, combined with the spectral range, imply that the resolution lens will require multiple elements to obtain good imaging characteristics, and warrant a custom design.

As outlined above, the design process of a wavelength-selective $1 \times K$ switch is straightforward. Given the switch requirements (number of output fibers, spectral equalization dynamic range, and channel passband characteristics), the optical param-

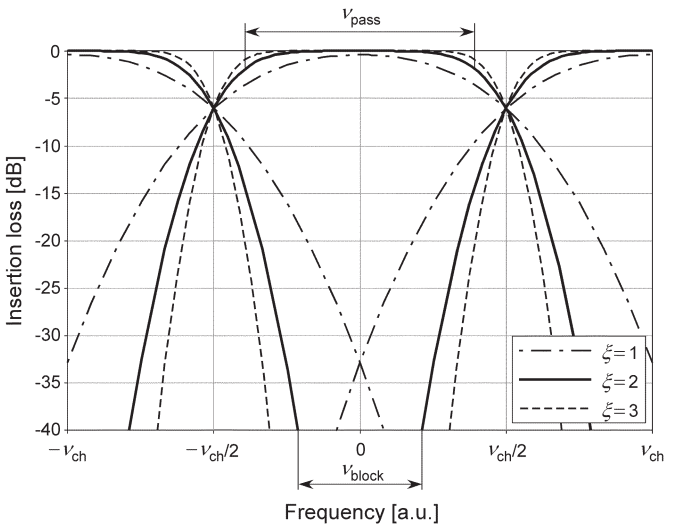

Fig. 5. Calculated passbands as a function of the confinement parameter ξ. Assumes a 100% fill-factor micromirror array, and effect of neighboring mirror is neglected. ξ is the ratio of mirror size to beam size and $\nu_{\rm ch}$ is the channel-to-channel frequency spacing.

and micromirror scan range, and confinement factor ξ, until a suitable design space is achieved. However, having so few critical parameters influencing the switch design is often too restrictive. We introduce anamorphic optics to obtain an additional design parameter that may lead to more efficient switch implementations.

C. Anamorphic Optics

The use of free-space optics in our switch design allows us to better utilize the three-dimensional volume of the switch package. We observe that the lenses' $F\#$ is determined by the extent of the linear array of $K+1$ beam apertures. In addition, the spectral resolution is determined by the magnified Gaussian beam width in the dispersion direction only. We introduce anamorphic optics to convert the circular Gaussian beam profiles to elliptical ones. The anamorphic optical elements are inserted into the first optical subassembly to generate a magnified elliptical beam whose narrow axis is in the spatial dispersion direction of the second optical subassembly. This ellipse orientation continues to satisfy the minimal beam size requirement for the spectral resolution.

The anamorphic elements are placed between the microlens array and the condenser lens, in the collimated beam region, and serve to compress the beams' vertical dimension by factor R. The fiber and microlens arrays are also both oriented vertically when employing the anamorphic optics (Fig. 6). Orienting the fiber array vertically means that the MEMS mirrors must tilt about an axis parallel to the dispersion direction. This is desirable for maximizing the channel passband [21] and reducing the sensitivity to mirror curvature [22]. The anamorphic effect reduces the extent of the $K+1$ beam apertures by R, increasing the condenser lens $F\#$ to

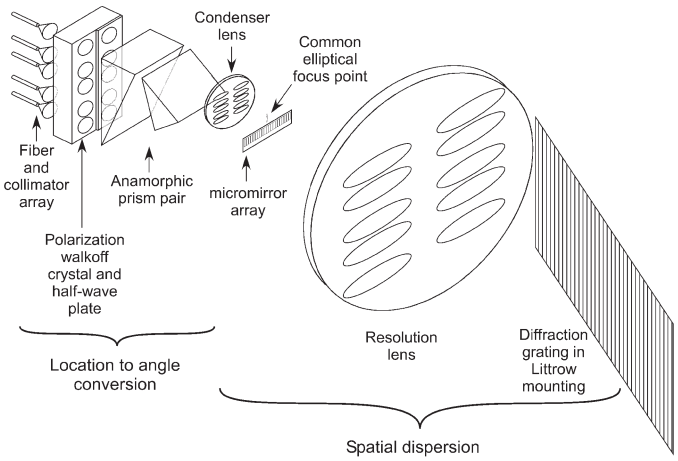

Fig. 6. Schematic of optical system showing the effect on beam size and shape of inserting anamorphic optics. The anamorphic optics ensures that high spectral resolution can be maintained while the apertures of the optics are minimized.

The benefit further extends to the $F\#$ of the resolution lens, as well as to the micromirror scan range, without effecting the confinement factor ξ. Therefore, we can now modify three parameters in order to reach a desirable switch design; the magnification ratio M and confinement ration ξ for determining the spectral resolution, and the anamorphic ratio R for controlling the lenses' $F\#$.

The advantages listed above may lead to a conclusion that the use of anamorphic optics is purely beneficial. However, the magnified elliptical beam requires the mirrors in the micromirror array to be longer by factor R. This can make the design of the MEMS mirrors more difficult since they are now longer in the direction of tilt, will have greater mass, and be more susceptible to curvature. Furthermore, the mirror resolution in tilt angle is also finer, requiring greater precision in mirror positioning.

III. Implementation of Wavelength-Selective $1 \times K$ Switches

We have realized three successful generations of wavelength-selective $1 \times K$ switches. These switches were designed to support the switching functionality, and provide wide and flat passbands for minimal signal filtering. Filtering is particularly critical since it is expected that signals will pass through multiple switches, and concatenated filtering will narrow the system passband [17], [23].

Common to all our switches is the support of a WDM system operating at the extended L-band (1554–1608 nm). Low insertion losses were achieved by using an 1100 lines/mm grating with high diffraction efficiency in the grating's S-plane [24] (polarization perpendicular to the groove direction), along with the aforementioned polarization diversity. The grating was Littrow-mounted at angle $\phi = 60.5^\circ$ (angle for center wavelength $\lambda_0 \sim 1582$ nm). The two logical subassemblies describe above were implemented as physical subassemblies, since this made

DOCKET ALARM

Explore Litigation Insights

Docket Alarm provides insights to develop a more informed litigation strategy and the peace of mind of knowing you're on top of things.

Real-Time Litigation Alerts

Keep your litigation team up-to-date with **real-time alerts** and advanced team management tools built for the enterprise, all while greatly reducing PACER spend.

Our comprehensive service means we can handle Federal, State, and Administrative courts across the country.

Advanced Docket Research

With over 230 million records, Docket Alarm's cloud-native docket research platform finds what other services can't. Coverage includes Federal, State, plus PTAB, TTAB, ITC and NLRB decisions, all in one place.

Identify arguments that have been successful in the past with full text, pinpoint searching. Link to case law cited within any court document via Fastcase.

Analytics At Your Fingertips

Learn what happened the last time a particular judge, opposing counsel or company faced cases similar to yours.

Advanced out-of-the-box PTAB and TTAB analytics are always at your fingertips.

API

Docket Alarm offers a powerful API (application programming interface) to developers that want to integrate case filings into their apps.

LAW FIRMS
Build custom dashboards for your attorneys and clients with live data direct from the court.

Automate many repetitive legal tasks like conflict checks, document management, and marketing.

FINANCIAL INSTITUTIONS
Litigation and bankruptcy checks for companies and debtors.

E-DISCOVERY AND LEGAL VENDORS
Sync your system to PACER to automate legal marketing.